HHS Public Access

Author manuscript

Mol Pharm. Author manuscript; available in PMC 2019 May 13.

Published in final edited form as:

Mol Pharm. 2018 September 04; 15(9): 3892–3900. doi:10.1021/acs.molpharmaceut.8b00359.

An indole-chalcone inhibits multidrug-resistant cancer cell growth by targeting microtubules

Hui Cong[a,1], **Xinghua Zhao**[b,c,1], **Brian T. Castle**[d], **Emily J. Pomeroy**[e], **Bo Zhou**[b], **John Lee**[f], **Yi Wang**[g], **Tengfei Bian**[g], **Zhenyuan Miao**[h], **Wannian Zhang**[a,h], **Yuk Yin Sham**[i], **David J. Odde**[d], **Craig E. Eckfeldt**[e], **Chengguo Xing**[a,b,g,**], and **Chunlin Zhuang**[a,h,*]

[a]School of Pharmacy, Ningxia Medical University, Yinchuan, China

[b]Department of Medicinal Chemistry, University of Minnesota, Minneapolis, MN, USA

[c]College of Veterinary Medicine, Hebei Agricultural University, Baoding, China

[d]Department of Biomedical Engineering, University of Minnesota, Minneapolis, MN, USA

[e]Department of Medicine, Division of Hematology, Oncology, and Transplantation, University of Minnesota, Minneapolis, MN, USA

[f]Department of Biochemistry, Molecular Biology and Biophysics, University of Minnesota, Minneapolis, MN, USA

[g]Department of Medicinal Chemistry, University of Florida, Gainesville, FL, USA

[h]School of Pharmacy, Second Military Medical University, Shanghai, China

[i]Department of Integrative Biology and Physiology, University of Minnesota, Minneapolis, MN, USA

Abstract

Multidrug resistance and toxic side effects are the major challenges in cancer treatment with microtubule-targeting agents (MTAs), and thus, there is an urgent clinical need for new therapies. Chalcone, a common simple scaffold found in many natural products, is widely used as a privileged structure in medicinal chemistry. We have previously validated tubulin as the anticancer target for chalcone derivatives. In this study, an α-methyl-substituted indole-chalcone (**FC77**) was synthesized and found to exhibit an excellent cytotoxicity against the NCI-60 cell lines (average concentration causing 50% growth inhibition = 6 nM). More importantly, several multidrug-resistant cancer cell lines showed no resistance to **FC77**, and the compound demonstrated good selective toxicity against cancer cells versus normal $CD34^+$ blood progenitor cells. A further mechanistic study demonstrated that **FC77** could arrest cells which relates to the binding to

[*]Corresponding author. School of Pharmacy, Ningxia Medical University, Yinchuan 750004, China. [**]Corresponding author. zclnathan@163.com (C. Zhuang), chengguoxing@cop.ufl.edu (C. Xing).</email>.

[1]Authors have contributed equally.

Conflicts of interest

The authors declare that they have no competing interests.

Supporting Information

Supplementary data related to this article can be found at http://dx.doi.org/###, including Structure-activity relationship, chalcone synthesis and characterization, docking studies, NCI60 panel data, spectra of synthesized compounds and references.

tubulin, and inhibit the microtubule dynamics. The National Cancer Institute COMPARE analysis and molecular modeling indicated that **FC77** had a mechanism of action similar to that of colchicine. Overall, our data demonstrate that this indole-chalcone represents a novel MTA template for further development of potential drug candidates for the treatment of multidrug-resistant cancers.

Graphical Abstract

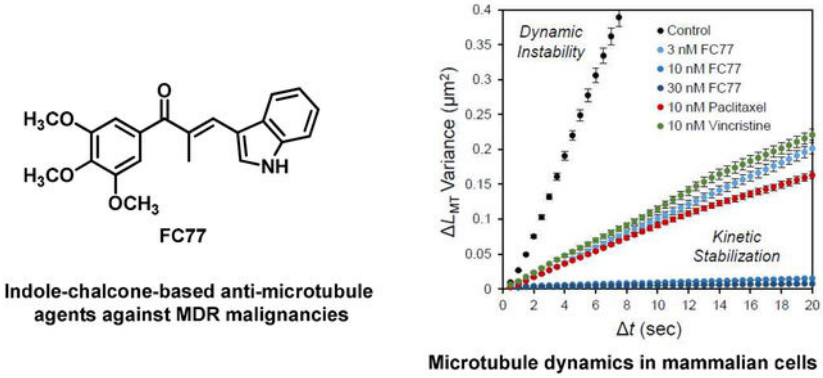

Keywords

Indole-chalcone; Multidrug resistance; Microtubule-targeting agent; Cancer

1. Introduction

Microtubules, composed of α- and β-tubulin heterodimers, are a validated druggable target for a number of marketed antitumor drugs (Fig. 1). The drugs are classified into two categories, microtubule-stabilizing agents (MSAs) and microtubule-destabilizing agents (MDAs)[1–3]. MSAs, such as paclitaxel (Taxol®) and ixabepilone, prevent microtubules disassembly, whereas MDAs, such as vinblastine and vincristine, inhibit microtubule polymerization. A new MDA from marine sponges, eribulin, has recently been approved for the treatment of breast cancer and liposarcoma[4]. Indeed, microtubule-targeting agents (MTAs) represent one of the most commonly used classes of chemotherapies in the treatment of cancer[5]. However, there is a high risk for cancer cells to acquire drug resistance during MTA treatment; consequently, tumors often reveal a multidrug-resistant (MDR) phenotype[6]. Cancer cells can acquire multidrug resistance via different mechanisms, including the overexpression of ATP-binding cassette (ABC) transporters. ABC transporters are overexpressed in ~40% of breast cancer patients, and the proportion can increase to ~70% upon chemotherapy treatment[7]. Toxic side effects are another challenge that limits the clinical use of MTAs[8]. Therefore, there is an urgent clinical need for new MTA anticancer agents, which would ideally be able to selectively target MDR malignancies while showing low toxicity for normal tissues.

Since substrates for ABC transporters are typically structurally complex, such as the clinical MTAs, anticancer agents with a simpler structure may offer a better opportunity to mitigate the risk of multidrug resistance. Chalcone is a simple and privileged structure in medicinal

chemistry, with diverse biological activities, including anticancer activity[9–11]. Recently, our group has demonstrated, via a whole-cell-based photoaffinity labeling approach, that tubulin is the direct cellular target of chalcones, responsible for their anticancer effects. A mass spectrometry-based approach has revealed that a positive chalcone probe modified the peptide N337-K350 (NSSYFVEWIPNNVK), suggesting targeting of the colchicine-binding site (Supplementary Fig. S1), which is different from the paclitaxel- or vinblastine-binding sites[12]. Molecular modeling of this probe showed that its azide group was within 2.2 Å and 2.5 Å of the labeled peptide (Supplementary Fig. S2). To date, no clinical MTA agents have been reported to target the colchicine-binding site as anticancer agents.

Based on these results and our earlier structure–activity relationship (SAR) data[13], seven indole-chalcones were developed and characterized in this study (Supplementary Table S1), and the lead compound (**FC77**; Fig. 2) was evaluated for its *in vitro* anticancer activity and the mechanism of action.

2. Materials and methods

2.1. Chemicals and reagents

All purchased reagents and solvents were used without further purification. Silica gel chromatography was performed on Whatman silica gel 60 Å (230–400 mesh). Nuclear magnetic resonance (NMR) spectra (^{1}H and 13C) were recorded on a spectrometer (Bruker Ascend 400) and calibrated using the deuterated solvent residual as an internal reference. High-resolution mass spectrometry (HRMS) was performed using a Q-TOF micro mass spectrometer. Compound **4** was analyzed by high-performance liquid chromatography (HPLC; Agilent 1100) using an Agilent Eclipse Plus C18 column (4.6 × 100 mm, 3.5 μm) and a 20-min linear gradient from 100% A (20 mM ammonium acetate, pH 6.8, in 10% CH_3CN) to 100% B (CH_3CN) at a flow rate of 1 mL/min. Purities of the other compounds were analyzed by HPLC (Agilent 1100) using an ODS-A column (YMC Pack; 10 × 250 mm, 5 μm) with methanol:H_2O (100:0 to 80:20 over 20 min and 80:20 thereafter) as the mobile phase with a flow rate of 2 mL/min. The separation was monitored at wavelengths of 254 and 365 nm. The purities of all final compounds were higher than 95%.

2.2. Synthesis of indole-chalcones

The synthetic route is presented in Supplementary Scheme S1 using two patents as references.[14, 15] To a solution of indole-3-carboxaldehyde (1 mmol) in ethanol (4 mL), piperidine (1.2 mmol) and the corresponding acetophenone (0.5 mmol) were added. After the mixture was stirred at 95 °C for 48 h, the reaction was quenched with hydrochloric acid diluted to pH 6 and then extracted with ethyl acetate. The organic layer was washed with aqueous $NaHCO_3$, water, and brine, then dried over anhydrous Na_2SO_4, and finally concentrated. The residue was recrystallized in ethanol at −20 °C for 24 h to afford the target compound **FC77**. Recrystallization yield: 8.2%. ^{1}H NMR (400MHz, $CDCl_3$): δ 8.71 (1H, br, NH), 7.69 (1H, s, Ar-H), 7.64 (1H, s, =CH), 7.59 (1H, d, J = 8.0 Hz, Ar-H), 7.45 (1H, d, J = 8.0 Hz, Ar-H), 7.30 (1H, d, J = 7.2 Hz, Ar-H), 7.22 (1H, t, J = 7.5 Hz, Ar-H), 7.03 (2H, s, Ar-H), 3.96 (3H, s, OCH_3), 3.89 (6H, s, $2OCH_3$), 2.32 (3H, s, CH_3). ^{13}C NMR (100MHz, $CDCl_3$): δ 197.98, 152.78, 135.46, 134.52, 131.76, 127.64, 125.93, 123.37, 121.04, 118.44,

113.31, 111.45, 106.94, 60.97, 56.26, 15.39. HRMS (ESI^+) m/z Calculated for $C_{21}H_{22}NO_4$ 352.1543; Observed 352.1543 ($M+H^+$). HPLC Purity: 97.4%, R_t = 35.70 min, UV 254 nm. The NMR, HRMS, and purity spectra are included in the Supplemental Information.

2.3. Cell lines and cell culture

Human A549, A549/T, A549/DDP, HCT-116, HCT-116/L, HL60, HL60/DOX, K562, K562/HHT300, CCRF-CEM, and CCRF-CEM/VLB100 cells were authenticated via DNA analysis by Genetica DNA Laboratories (Cincinnati, OH, USA) or by the University of Arizona Genomics Core. Cells were cultured following our standard protocols[12, 13, 16–20] and tested monthly for *Mycoplasma* contamination. De-identified mobilized peripheral blood (MPB) was obtained after informed consent according to protocols approved by the University of Minnesota Institutional Review Board.

K562 and K562/HHT300 cell lines were provided by Dr. Tang.[21] K562/HHT300 was developed from K562 upon chronic exposure to homoharringtonine, a protein translation inhibitor. HL60 and HL60/DOX cell lines were provided by Dr. Ganapathi.[22] HL60/DOX was developed from HL60 upon chronic exposure to doxorubicin (a topoisomerase inhibitor). CCRF-CEM and CCRF-CEM/VLB100 were provided by Dr. Beck[23, 24]. CCRF-CEM/VLB100 was developed from CCRF-CEM upon chronic exposure to vinblastine, an antimicrotubule agent. A549, A549/T, A549/DDP, HCT-116 and HCT-116/L were obtained from State Key Laboratory of Oncogenes and Related Genes, Cancer Institute of Shanghai Jiaotong University. A549/T and A549/DDP were developed from A549 upon chronic exposure to paclitaxel and cisplatin, respectively. HCT-116/L was developed from HCT-116 upon chronic exposure to oxaliplatin. We have evaluated all the parental cell lines and the MDR cell lines, using the names as in their original reports. Comparison has been made only between the MDR cell line with its corresponding parental cell line.

2.4. Cell viability measurement

In vitro cytotoxicity of the compounds was assayed by determining their ability to inhibit the growth of tumor cells. In brief, cells were plated in a 96-well plate (at a density of ~4,000 cells/well for adherent cells and ~10,000 cells/well for suspension cells). The cells were treated with a series of dilutions of the test compounds, with the final concentration of dimethyl sulfoxide (DMSO) of 1% in the cell medium; cells treated with medium containing 1% DMSO served as a control. After a 48- or 72-h treatment, the relative cell viability in each well was determined using a CellTiter-Blue cell viability assay kit. The concentration causing 50% inhibition of the cell growth (GI_{50}) of each candidate compound was determined by fitting the relative cell viability to the drug concentration using a dose-response model in the GraphPad Prism program (GraphPad Software, San Diego, CA, USA). For the National Cancer Institute (NCI)-60 screening panel, the treatment lasted for 72 h.

2.5. Colony formation assay

Cells (100 cells per condition for leukemia cell lines or 500 cells per condition for MPB) were treated with doxorubicin, vincristine, or **FC77** for 24 h in a standard culture medium and then harvested and plated in MethoCult H4034 optimum CFC medium (Stem Cell

Technologies) according to the manufacturer's recommendations. Colonies were scored after 7–14 days under an inverted microscope.

2.6. Analysis of cell-cycle distribution by flow cytometry

The cell cycle was analyzed by flow cytometry based on the DNA content following our established procedures[13, 25], with slight modifications. Briefly, HL60 cells (10^6 cells/mL) or HCT116 cells ($5*10^5$ cells/mL) were treated with compounds at their corresponding GI_{50} concentrations with 1% DMSO for different time points (1–12 h). The cells were then washed twice with ice-cold phosphate-buffered saline (PBS) and resuspended in 1 mL of PBS. The suspension was mixed with cold 70% ethanol (9 mL) and fixed at 4 °C overnight. Cell pellets were collected by centrifugation, washed twice with PBS, then resuspended in 1 mL of a propidium iodide (PI) staining solution (50 μg/mL PI, 200 μg/mL RNase A, and 0.1% Triton X-100 in PBS), and incubated at room temperature for 30 min in the dark. The cell-cycle distribution was then analyzed using a BD FACSCalibur flow cytometer.

2.7. Differential scanning fluorimetry assay

Briefly, a tubulin monomer was mixed with colchicine, paclitaxel, vinblastine or **FC77** (50 μM) in the presence of GDP (0.1 mg/mL), and the melting temperature of tubulin was measured using BioRad CFX96 Real-Time PCR System following established procedures[26, 27].

2.8. Microtubule dynamics

The individual microtubule dynamics were measured in the presence of MTAs and analyzed as described previously[28]. Briefly, LLC-PK1 porcine kidney cells, stably expressing enhanced green fluorescent protein (EGFP)–tubulin, were treated with Taxol (Sigma–Aldrich, St. Louis, MO, USA), vincristine sulfate (Sigma), or **FC77** for 30 min prior to imaging. A total of 121 frames were collected every 0.5 s for 60 s, while the lengths of individual microtubules were determined using the TipTracker software without modification[29].

2.9. Statistical analysis

The *in vitro* cytotoxicity assay was performed at least three times in triplicate. Comparisons were made using a two-tailed Student's *t*-test. A value of $p \leq 0.05$ was considered statistically significant.

3. Results

3.1. FC77 shows strong cytotoxicity against NCI-60 cancer cell lines

The NCI-60 human cancer cell line screening has been widely used to identify potential anticancer drug candidates, to help elucidate the mechanism of action, and to help prioritize the types of malignancies for the development[30]. Through this screening, **FC77** was found to be a low-nanomolar inhibitor of the growth of the majority of the NCI-60 human cancer cell lines (average GI_{50}: ~6 nM; Table 1 and Supplementary Fig. S4), with some preference

toward leukemia, colon, and central nervous system cancers (GI_{50} < 4 nM for all 19 cell lines), as well as toward non-small-cell lung cancers, with only one exception (HOP-92).

3.2. FC77 inhibits the growth of multiple parental and corresponding MDR cancer cells

We further explored the anticancer potential of **FC77** against leukemia (HL60 vs. HL60/DOX, K562 vs. K562/HHT300, CCRF-CEM vs. CCRF-CEM/VLB100), non-small-cell lung cancer (A549 vs. A549/T and A549/DDP), and colon cancer (HCT-116 vs. HCT-116/L) cell lines and their corresponding MDR counterparts.

The drug-resistant cell lines all demonstrated MDR phenotypes, as shown for paclitaxel and vinblastine (Supplementary Fig. S5), potentially via upregulation of ABC transporters[18]. Unlike paclitaxel and vinblastine, **FC77** retained its cytotoxicity against the MDR cancer cell lines, with the GI_{50} values of 1–53.4 nM (Fig. 3). Although **FC77** did not reveal selectivity toward A549/T cells (GI_{50} = 53.4 ± 1.1 nM), it was much more potent than paclitaxel (GI_{50} = 2,090 ± 64 nM; Supplementary Fig. S5) against this cell line. For parental CCRF-CEM and HCT-116 cells and their resistant derivatives, **FC77** showed less selectivity; however, the GI_{50} values were in the low nanomolar range (1–8 nM). Moreover, K562/HHT300 and, particularly, HL60/DOX and A549/DDP cells were more sensitive to **FC77** than their parental cells, suggesting the potential of **FC77** to treat MDR malignancies as a complementary treatment to the current standard chemotherapies.

3.3. FC77 shows a safer therapeutic window and low toxic side effects

The differential anticancer activity of **FC77** against HL60 and HL60/DOX cells was further evaluated by a colony formation assay (Fig. 4), which reflects their leukemic stem cell activity. The clonogenic potential of HL60 and HL60/DOX cells was significantly and dose-dependently reduced upon treatment with this indole-chalcone. **FC77** was more active against drug-resistant HL60/DOX cells than against HL60 cells in the colony formation assay. A significant difference was observed at a low drug concentration (0.01 μM). As expected, conventional chemotherapeutic agents (doxorubicin and vincristine) were highly active against HL60 cells but much less effective against the resistant HL60/DOX cell line. To evaluate the potential therapeutic window of **FC77**, we also evaluated its effects on colony formation by normal $CD34^+$ blood progenitor cells derived from MPB of healthy donors[31]. While doxorubicin and vincristine showed a greater inhibitory effect on the colony formation by normal MPB cells than on that by MDR HL60/DOX cells, **FC77** was markedly less toxic to normal MPB cells than to MDR HL60/DOX leukemia cells (Fig. 4), which suggests its safer therapeutic window and translational potential.

3.4. FC77 significantly induces cell cycle arrest

We then characterized the impact of **FC77** and three standard drugs (doxorubicin, paclitaxel, and vinblastine) on the HL60 cell-cycle distribution. The concentrations of the compounds were equal to their corresponding 48-h GI_{50}s. The cells treated with **FC77** showed a significantly larger population in the G2/M phase than the control cells (Fig. 5A). Vinblastine also significantly induced cell cycle arrest, while paclitaxel slightly increased the G2/M population, consistent with their antimicrotubule mechanisms of action. Doxorubicin showed no induction of cell cycle arrest. Given that FC77 showed the impact on cell cycle,

we further evaluated its effects toward HL60 and HCT116 using different time points (Fig. 5B and C). **FC77** can arrest these two cells in a significant time-dependent manner. The HL60 cells showed the population of ~14–25% in the G2/M phase. HCT116 cells can be arrested in the G2/M phase from ~25% at 1h to ~60 % at 12 h.

3.5. FC77 directly interacts with tubulin

We next explored the ability of **FC77** to directly interact with tubulin by measuring its effect on the melting temperature of tubulin by differential scanning fluorimetry[27]. As shown in Fig. 6, colchicine and vinblastine increased the melting temperature by 3 and 2 °C, respectively, while paclitaxel increased the temperature by only 1 °C. We speculated that the weak effect of paclitaxel could be due to its preferential interaction with microtubules, instead of tubulin. **FC77** increased the melting temperature by 4 °C, i.e., more than the three standard MTAs, indicating its direct interaction with tubulin.

3.6. FC77 significantly blocks the dynamics of individual microtubules

The effect of **FC77** on the microtubule dynamics was characterized via direct imaging of microtubule dynamics in intact LLC-PK1 porcine kidney cells (Fig. 7). Normally, microtubules in intact cells undergo dynamic changes via polymerization and depolymerization, exhibiting a high assembly variance over time (DMSO control in Fig. 7A). As expected, paclitaxel and vincristine (10 nM) significantly reduced the dynamics of individual microtubules. A similar reduction was achieved with **FC77** when its concentration was 3 nM (Fig. 7A). However, **FC77** completely blocked the microtubule dynamics when its concentration reached 10 nM (Fig. 7A, B, and D). A dose-response quantitative analysis showed that **FC77** was a more potent inhibitor than paclitaxel and vincristine. The half-maximal inhibitory concentration (IC_{50}) was approximately 3 nM for **FC77** compared to 14 nM and 37 nM for paclitaxel and vincristine, respectively (Fig. 7C).

3.7. FC77 shows a similar microtubule-depolymerizing mechanism with that of colchicine

To confirm the antimicrotubule mechanism of **FC77**, we used the NCI COMPARE algorithm to compare the **FC77** activity profile with those of other anticancer therapeutics. The similarity relative to **FC77** was expressed using a Pearson's correlation coefficient (PCC). A PCC value of > 0.5 is generally considered significant[32, 33]. Our COMPARE analysis results showed that **FC77** was similar in its mechanism of action to five representative antimicrotubule agents (Table 2). Colchicine, in particular, showed a PCC value of 0.658 relative to **FC77**, indicating a similar microtubule-depolymerizing mechanism, while **FC77** was approximately 10-fold more potent than colchicine (average GI_{50} = 57.5 nM in the NCI database)[34]. Additionally, colchicine was not highly active against HL60/DOX cells (GI_{50} = 10.3 μM), which showed a 25-fold higher resistance than that of parental HL60 cells (Supplementary Fig. S7).

4. Discussion

Chalcone is a privileged structure in medicinal chemistry because it shows diverse biological activities, including anticancer activity[9]. Nevertheless, there is not enough convincing evidence to confirm its anticancer binding targets. In our previous study, we have

unambiguously confirmed β-tubulin as a direct cellular target of chalcones via whole-cell-based photoaffinity[12]. The results prompted us to investigate drug candidates based on the chalcone scaffold and their molecular mechanisms.

FC77, an indole-chalcone derivative, was demonstrated to show marked potency against multiple cancer cell lines by targeting microtubules. Since multidrug resistance is a major challenge for clinical MTA cancer treatment, our findings suggest the potential of **FC77** to mitigate this clinical issue. The potential advantage of **FC77** is its simple structure compared with those of complex clinical antimicrotubule agents. Combretastatin A-4, a natural product from *Combretum caffrum*[35] and an MTA with a simple structure similar to that of **FC77**, were evaluated in parallel and found to have a similar selectivity profile and potencies (Supplementary Fig. S6), indicating that MTAs with simple structures may be useful for treating MDR malignancies. Moreover, it is reported that tubulin binding agents that specifically target the colchicine binding site may circumvent the MDR[36, 37]. Thus, several experiments were then applied to support its colchicine-binding property.

The cell cycle arrest is a key feature of antimicrotubule agent-induced cytotoxicity[38, 39]. Apoptosis, on the other hand, can be induced by therapeutic agents with various mechanisms of action, making it difficult to understand the upstream mechanisms. Thus, the increased G2/M phase population in two cell lines after treatment with **FC77** suggested that **FC77** induced the arrest at G2 and/or M phase. Additional data, including the melting temperature (biochemical binding), COMPARE (correlative analysis), and molecular modeling (Supplementary Figs. S1–S3) data, as well as our previous whole-cell-based photoaffinity labeling data[12], collectively support this mechanism of action. A whole-cell microtubule dynamics assay was used, instead of a tubulin polymerization/depolymerization biochemical assay, to confirm the direct interaction of **FC77** with tubulin, mainly because the concentrations needed to induce polymerization or depolymerization could be more than 1,000-fold higher than cytotoxic concentrations and because there might be a limited correlation, if any, between the biochemical potency and *in vitro* cytotoxicity, as has been reported for tubulysin by Fecik et al.[40]. Besides, molecular modeling showed that the compound could be well docked into the colchicine-binding site, and a good superposition with colchicine was observed. A clear SAR (Supplemental Information), with a decent correlation ($R^2 = 0.70$) between the GI_{50} values of the compounds and their activities predicted by an atom-based QSAR model, was also obtained (Supplementary Fig. S3C). The 5-methoxyl and 1-amino functional groups of **FC77** interacted with Cys241 and Asn101 of tubulin via hydrogen bonding (Supplementary Fig. S3A and B), consistent with the potent cytotoxicity of the compound.

There have been some concerns about the chalcone template because it contains a pan-assay-interference-compounds (PAINS) fragment[41, 42]. However, the use of PAINS as a filter has been challenged[43, 44]. Compounds with a potentially promiscuous template must be carefully evaluated before they are excluded. In this study, the effect of **FC77** on microtubule dynamics in intact cells was characterized, and the compound was demonstrated to completely inhibit the microtubule dynamics when its concentration reached 10 nM, which is much lower than the typical concentrations for PAINS effects. A dose-response quantitative analysis showed that **FC77** is a more potent inhibitor of microtubule dynamics

than are paclitaxel and vincristine. Besides, our previous data also support β-tubulin as a direct cellular target of chalcones[12]. Collectively, these studies demonstrated that the reported compounds possess specific activities and their apparent activity is not an artifact due to the PAINS potential.

In summary, we synthesized a series of chalcone compounds, for which a clear SAR was demonstrated, with a good correlation with their modeled binding interactions with tubulin. **FC77** exhibited excellent cytotoxicity against the NCI-60 human cancer cell lines, with the GI_{50} values in the low nanomolar range. A mechanistic study demonstrated that **FC77** arrested the cell cycle which might relate to the binding to tubulin, and inhibited the microtubule dynamics. The COMPARE analysis indicated that **FC77** had a mechanism of action similar to that of colchicine and other MTAs. These data consistently support the antimicrotubule mechanism of action of **FC77**. More importantly, MDR cancer cell lines showed no resistance to **FC77**, and this compound demonstrated selective cytotoxicity against cancer cells, with less toxicity against normal $CD34^+$ blood progenitor cells. Overall, our data show that **FC77** represents a novel MTA template for drug development to treat MDR cancers.

Supplementary Material

Refer to Web version on PubMed Central for supplementary material.

Acknowledgements

This research was funded by grants from the Shanghai Municipal Commission of Health and Family Planning (2017YQ052 to C.Z.); the Young Elite Scientists Sponsorship Program by the China Association for Science and Technology (2017QNRC061 to C.Z.); the Key Research and Development Program of Ningxia (2018BFH02001 to W. Z. and 2018BFH02001–01 to C.Z.); the Shanghai “ChenGuang” Project (16CG42 to C.Z.); the National Natural Science Foundation of China (81502978 to C.Z.); the National Cancer Institute, National Institutes of Health, USA (R01CA163864 to C.X.); Ningxia Medical University (XT2017022 to C.X.); the University of Minnesota Masonic Cancer Center and Academic Health Center Heme Malignancy Tissue Bank; and the National Heart, Lung, and Blood Institute, National Institutes of Health, USA (T32HL007062 to C.E.E.). We also thank Dr. Li Su for the cell cycle analysis.

References

1. Chen SM; Meng LH; Ding J New microtubule-inhibiting anticancer agents. Expert Opin. Investig. Drugs 2010, 19, (3), 329–343.
2. Gigant B; Wang C; Ravelli RB; Roussi F; Steinmetz MO; Curmi PA; Sobel A; Knossow M Structural basis for the regulation of tubulin by vinblastine. Nature 2005, 435, (7041), 519–522. [PubMed: 15917812]
3. Li W Drugs targeting tubulin polymerization. Pharm. Res 2012, 29, (11), 2939–2942. [PubMed: 23054091]
4. https://www.clinicaltrials.gov/ct2/results?term=eribulin+OR+E7389.
5. Dumontet C; Jordan MA Microtubule-binding agents: a dynamic field of cancer therapeutics. Nat. Rev. Drug Discov 2010, 9, (10), 790–803. [PubMed: 20885410]
6. Kavallaris M Microtubules and resistance to tubulin-binding agents. Nat. Rev. Cancer 2010, 10, (3), 194–204. [PubMed: 20147901]
7. Fletcher JI; Haber M; Henderson MJ; Norris MD ABC transporters in cancer: more than just drug efflux pumps. Nat. Rev. Cancer 2010, 10, (2), 147–156. [PubMed: 20075923]
8. Wieczorek M; Tcherkezian J; Bernier C; Prota AE; Chaaban S; Rolland Y; Godbout C; Hancock MA; Arezzo JC; Ocal O; Rocha C; Olieric N; Hall A; Ding H; Bramoulle A; Annis MG;

Zogopoulos G; Harran PG; Wilkie TM; Brekken RA; Siegel PM; Steinmetz MO; Shore GC; Brouhard GJ; Roulston A The synthetic diazonamide DZ-2384 has distinct effects on microtubule curvature and dynamics without neurotoxicity. Sci. Transl. Med 2016, 8, (365), 365ra159.

9. Zhuang C; Zhang W; Sheng C; Zhang W; Xing C; Miao Z Chalcone: A Privileged Structure in Medicinal Chemistry. Chem Rev 2017, 117, (12), 7762–7810. [PubMed: 28488435]
10. Singh P; Anand A; Kumar V Recent developments in biological activities of chalcones: a mini review. Eur. J. Med. Chem 2014, 85, 758–777. [PubMed: 25137491]
11. Zhou B; Xing C Diverse Molecular Targets for Chalcones with Varied Bioactivities. Med. Chem. (Los Angeles) 2015, 5, (8), 388–404. [PubMed: 26798565]
12. Zhou B; Yu X; Zhuang C; Villalta P; Lin Y; Lu J; Xing C Unambiguous Identification of beta-Tubulin as the Direct Cellular Target Responsible for the Cytotoxicity of Chalcone by Photoaffinity Labeling. ChemMedChem 2016, 11, (13), 1436–1445. [PubMed: 27203512]
13. Zhou B; Jiang P; Lu J; Xing C Characterization of the Fluorescence Properties of 4-Dialkylaminochalcones and Investigation of the Cytotoxic Mechanism of Chalcones. Arch. Pharm. (Weinheim) 2016, 349, (7), 539–552. [PubMed: 27214789]
14. Kyowa H; K.K. K Propenone derivatives Europe Patent 0680950A1, 1994.
15. Kyowa H; K.K. K Propenone derivatives. U.S. Patent 5952355A, 1995.
16. Zhang Y; Srinivasan B; Xing C; Lu J A new chalcone derivative (E)-3-(4-methoxyphenyl)-2-methyl-1-(3,4,5-trimethoxyphenyl)prop-2-en-1-one suppresses prostate cancer involving p53-mediated cell cycle arrests and apoptosis. Anticancer Res. 2012, 32, (9), 3689–3698. [PubMed: 22993307]
17. Srinivasan B; Johnson TE; Lad R; Xing C Structure-activity relationship studies of chalcone leading to 3-hydroxy-4,3',4',5'-tetramethoxychalcone and its analogues as potent nuclear factor kappaB inhibitors and their anticancer activities. J. Med. Chem 2009, 52, (22), 7228–7235. [PubMed: 19883086]
18. Das SG; Hermanson DL; Bleeker N; Lowman X; Li Y; Kelekar A; Xing C Ethyl 2-amino-6-(3,5-dimethoxyphenyl)-4-(2-ethoxy-2-oxoethyl)-4H-chromene-3-carboxylate (CXL017): a novel scaffold that resensitizes multidrug resistant leukemia cells to chemotherapy. ACS Chem. Biol 2013, 8, (2), 327–335. [PubMed: 23102022]
19. Das SG; Srinivasan B; Hermanson DL; Bleeker NP; Doshi JM; Tang R; Beck WT; Xing C Structure-activity relationship and molecular mechanisms of ethyl 2-amino-6-(3,5-dimethoxyphenyl)-4-(2-ethoxy-2-oxoethyl)-4H-chromene-3-carboxylate (CXL017) and its analogues. J. Med. Chem 2011, 54, (16), 5937–5948. [PubMed: 21780800]
20. Aridoss G; Zhou B; Hermanson DL; Bleeker NP; Xing C Structure-activity relationship (SAR) study of ethyl 2-amino-6-(3,5-dimethoxyphenyl)-4-(2-ethoxy-2-oxoethyl)-4H-chromene-3-carboxylate (CXL017) and the potential of the lead against multidrug resistance in cancer treatment. J. Med. Chem 2012, 55, (11), 5566–5581. [PubMed: 22582991]
21. Tang R; Cohen S; Perrot JY; Faussat AM; Zuany-Amorim C; Marjanovic Z; Morjani H; Fava F; Corre E; Legrand O; Marie JP P-gp activity is a critical resistance factor against AVE9633 and DM4 cytotoxicity in leukaemia cell lines, but not a major mechanism of chemoresistance in cells from acute myeloid leukaemia patients. BMC Cancer 2009, 9, 199. [PubMed: 19549303]
22. Vaziri SA; Grabowski DR; Tabata M; Holmes KA; Sterk J; Takigawa N; Bukowski RM; Ganapathi MK; Ganapathi R c-IAP1 is overexpressed in HL-60 cells selected for doxorubicin resistance: effects on etoposide-induced apoptosis. Anticancer Res. 2003, 23, (5A), 3657–3661. [PubMed: 14666661]
23. Chen M; Beck WT DNA topoisomerase II expression, stability, and phosphorylation in two VM-26-resistant human leukemic CEM sublines. Oncol. Res 1995, 7, (2), 103–111. [PubMed: 7579726]
24. Beck WT; Mueller TJ; Tanzer LR Altered surface membrane glycoproteins in Vinca alkaloid-resistant human leukemic lymphoblasts. Cancer Res. 1979, 39, (6 Pt 1), 2070–2076. [PubMed: 571759]
25. Cao D; Han X; Wang G; Yang Z; Peng F; Ma L; Zhang R; Ye H; Tang M; Wu W; Lei K; Wen J; Chen J; Qiu J; Liang X; Ran Y; Sang Y; Xiang M; Peng A; Chen L Synthesis and biological

evaluation of novel pyranochalcone derivatives as a new class of microtubule stabilizing agents. Eur. J. Med. Chem 2013, 62, 579–589. [PubMed: 23425970]

26. Cala O; Remy MH; Guillet V; Merdes A; Mourey L; Milon A; Czaplicki G Virtual and biophysical screening targeting the gamma-tubulin complex--a new target for the inhibition of microtubule nucleation. PloS one 2013, 8, (5), e63908. [PubMed: 23691113]
27. Zhuang C; Narayanapillai S; Zhang W; Sham YY; Xing C Rapid identification of Keap1-Nrf2 small-molecule inhibitors through structure-based virtual screening and hit-based substructure search. J. Med. Chem 2014, 57, (3), 1121–1126. [PubMed: 24417449]
28. Castlea BT; McCubbinb S; Prahla LS; Bernensa JN; Septb D; Oddea DJ Mechanisms of kinetic stabilization by the drugs paclitaxel and vinblastine. Mol. Biol. Cell 2017, 28, (9), 1238–1257. [PubMed: 28298489]
29. Prahl LS; Castle BT; Gardner MK; Odde DJ Quantitative analysis of microtubule self-assembly kinetics and tip structure. Methods Enzymol. 2014, 540, 35–52. [PubMed: 24630100]
30. Shoemaker RH The NCI60 human tumour cell line anticancer drug screen. Nat. Rev. Cancer 2006, 6, (10), 813–823. [PubMed: 16990858]
31. Bhatia S; Reister S; Mahotka C; Meisel R; Borkhardt A; Grinstein E Control of AC133/CD133 and impact on human hematopoietic progenitor cells through nucleolin. Leukemia 2015, 29, (11), 2208–2220. [PubMed: 26183533]
32. Naasani I; Seimiya H; Yamori T; Tsuruo T FJ5002: a potent telomerase inhibitor identified by exploiting the disease-oriented screening program with COMPARE analysis. Cancer Res. 1999, 59, (16), 4004–4011. [PubMed: 10463599]
33. Yamori T; Matsunaga A; Sato S; Yamazaki K; Komi A; Ishizu K; Mita I; Edatsugi H; Matsuba Y; Takezawa K; Nakanishi O; Kohno H; Nakajima Y; Komatsu H; Andoh T; Tsuruo T Potent antitumor activity of MS-247, a novel DNA minor groove binder, evaluated by an in vitro and in vivo human cancer cell line panel. Cancer Res. 1999, 59, (16), 4042–4049. [PubMed: 10463605]
34. https://dtp.cancer.gov/dtpstandard/servlet/MeanGraph?searchtype=NSC&searchlist=757&outputformat=HTML&outputmedium=page&chemnameboolean=AND&debugswitch=false&assaytype=&testshortname=&dataarraylength=75&endpt=GI50&button=Mean+Graph&highconc=−4.0
35. Lee L; Robb LM; Lee M; Davis R; Mackay H; Chavda S; Babu B; O'Brien EL; Risinger AL; Mooberry SL; Lee M Design, synthesis, and biological evaluations of 2,5-diaryl-2,3-dihydro-1,3,4-oxadiazoline analogs of combretastatin-A4. J. Med. Chem 2010, 53, (1), 325–334. [PubMed: 19894742]
36. Arnst KE; Wang Y; Hwang DJ; Xue Y; Costello T; Hamilton D; Chen Q; Yang J; Park F; Dalton JT; Miller DD; Li W A Potent, Metabolically Stable Tubulin Inhibitor Targets the Colchicine Binding Site and Overcomes Taxane Resistance. Cancer Res. 2018, 78, (1), 265–277. [PubMed: 29180476]
37. Nguyen TL; Cera MR; Pinto A; Lo Presti L; Hamel E; Conti P; Gussio R; De Wulf P Evading Pgp activity in drug-resistant cancer cells: a structural and functional study of antitubulin furan metotica compounds. Mol. Cancer Ther 2012, 11, (5), 1103–1111. [PubMed: 22442310]
38. Zhu C; Zuo Y; Wang R; Liang B; Yue X; Wen G; Shang N; Huang L; Chen Y; Du J; Bu X Discovery of potent cytotoxic ortho-aryl chalcones as new scaffold targeting tubulin and mitosis with affinity-based fluorescence. J. Med. Chem 2014, 57, (15), 6364–6382. [PubMed: 25061803]
39. Shen KH; Chang JK; Hsu YL; Kuo PL Chalcone arrests cell cycle progression and induces apoptosis through induction of mitochondrial pathway and inhibition of nuclear factor kappa B signalling in human bladder cancer cells. Basic & Clin. Pharmacol. Toxicol 2007, 101, (4), 254–261.
40. Balasubramanian R; Raghavan B; Begaye A; Sackett DL; Fecik RA Total synthesis and biological evaluation of tubulysin U, tubulysin V, and their analogues. J. Med. Chem 2009, 52, (2), 238–240. [PubMed: 19102699]
41. Baell JB Feeling Nature's PAINS: Natural Products, Natural Product Drugs, and Pan Assay Interference Compounds (PAINS). J. Nat. Prod 2016, 79, (3), 616–628. [PubMed: 26900761]

42. Gilberg E; Gutschow M; Bajorath J X-ray Structures of Target-Ligand Complexes Containing Compounds with Assay Interference Potential. J. Med. Chem 2018, 61, (3), 1276–1284. [PubMed: 29328660]

43. Senger MR; Fraga CA; Dantas RF; Silva FP Jr. Filtering promiscuous compounds in early drug discovery: is it a good idea? Drug Discov. Today 2016, 21, (6), 868–872. [PubMed: 26880580]

44. Meng N; Tang H; Zhang H; Jiang C; Su L; Min X; Zhang W; Zhang H; Miao Z; Zhang W; Zhuang C Fragment-growing guided design of Keap1-Nrf2 protein-protein interaction inhibitors for targeting myocarditis. Free Radic. Biol. Med 2018, 117, 228–237. [PubMed: 29428410]

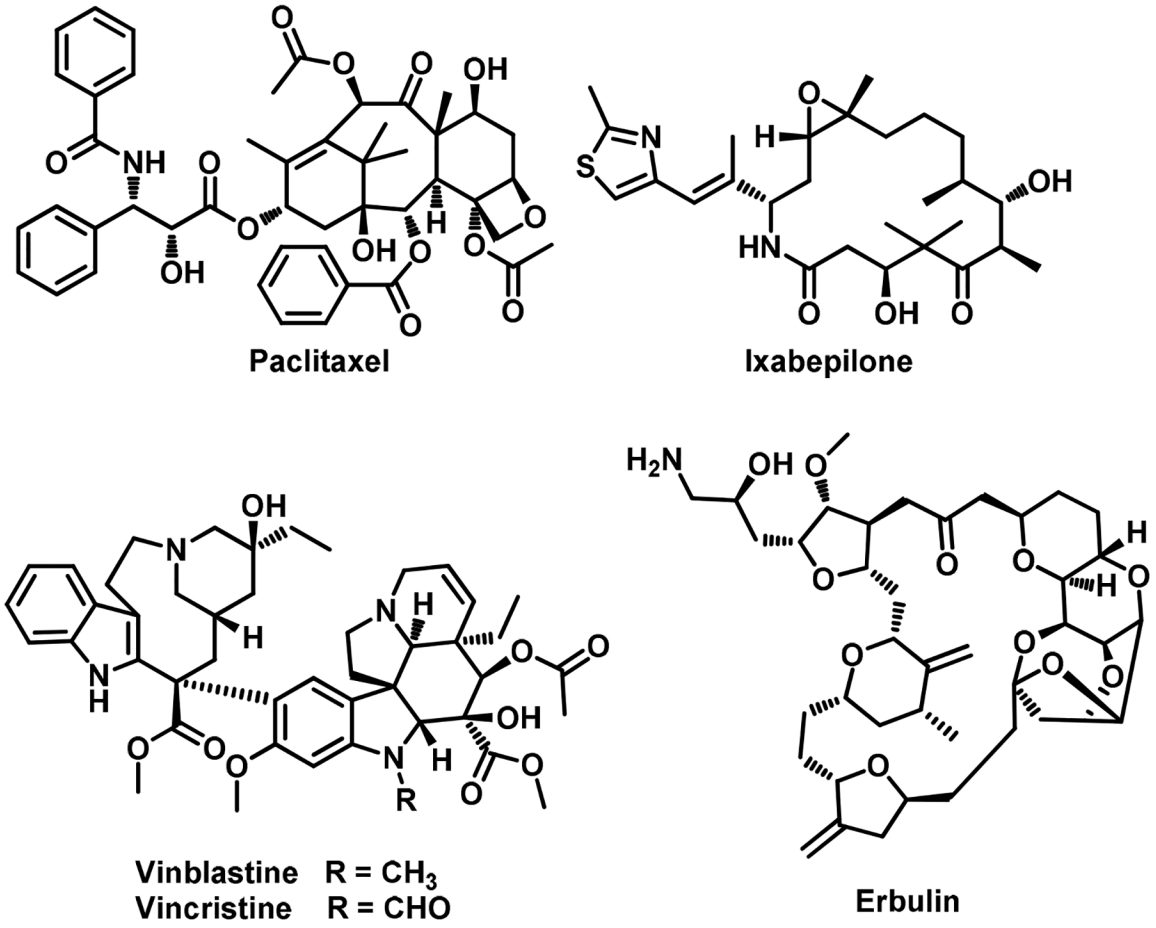

Fig. 1.
Representative antimicrotubule cancer therapeutic drugs.

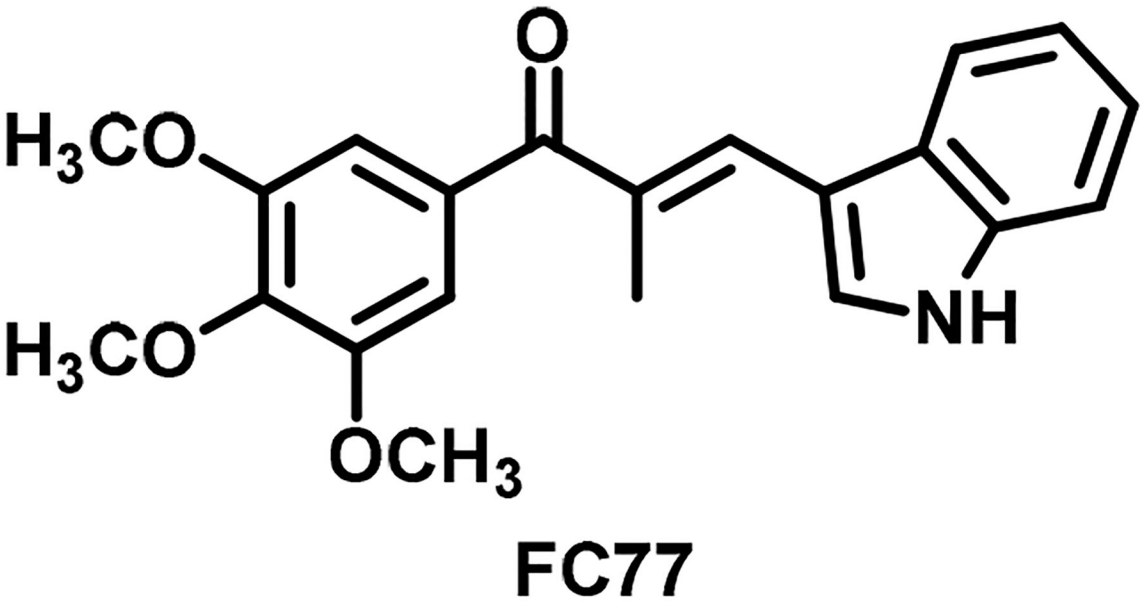

Fig. 2.
Chemical structure of the novel indole-chalcone **FC77**.

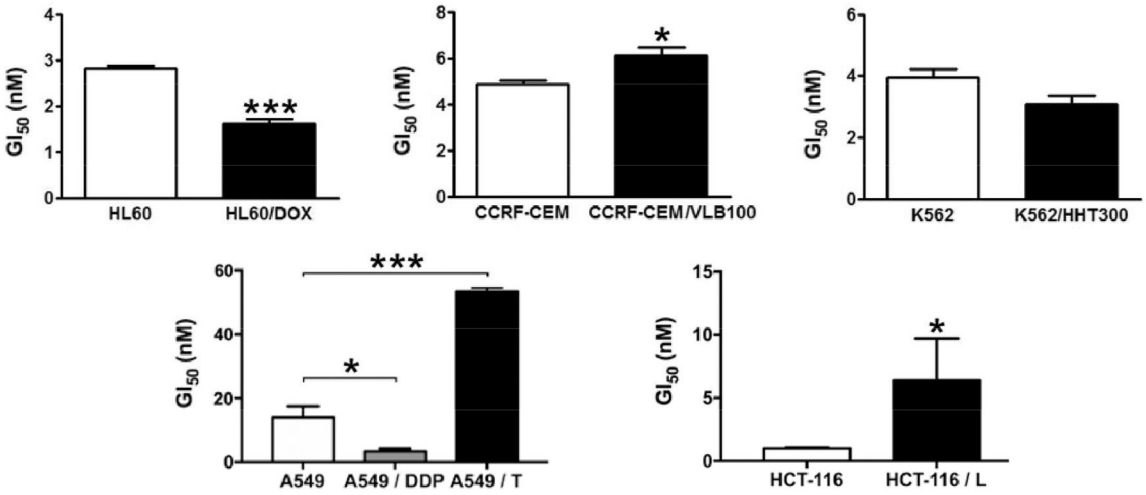

Fig. 3.

Comparison of cytotoxicity of **FC77** against multidrug-resistant cancer cell lines and their parental cancer cell lines. *p < 0.05, ***p < 0.001.

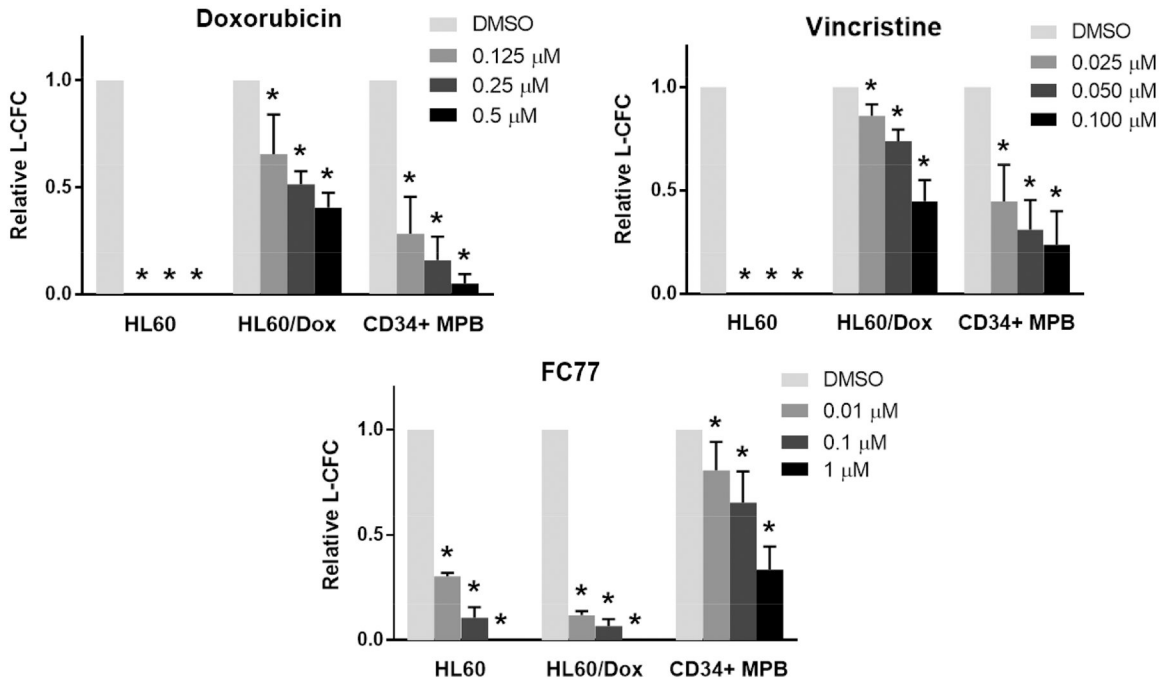

Fig. 4.

Preferential cytotoxicity of **FC77** to HL60/DOX cells over HL60 cells, and its therapeutic window for $CD34^+$ MPB cells, assessed via a leukemia colony-forming cell (L-CFC) assay. Cells (100 cells per condition for leukemia cell lines or 500 cells per condition for MPB) were treated with doxorubicin, vincristine, or FC77 for 24 h in a standard culture medium and then harvested and plated in MethoCult H4034 optimum CFC medium (Stem Cell Technologies) according to the manufacturer's recommendations. Colonies were scored after 7–14 days under an inverted microscope. *$p < 0.05$.

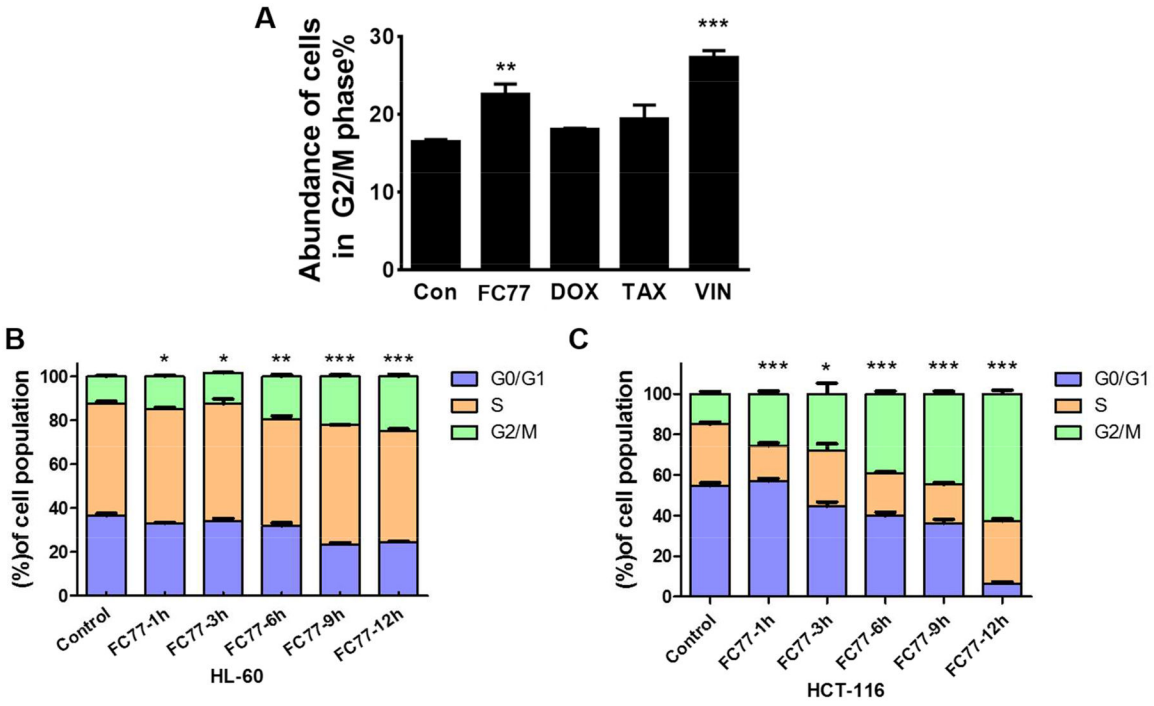

Fig. 5.

(A) Effects of **FC77** and standard therapeutic drugs on the HL60 cell cycle upon a 6-h treatment. DOX, doxorubicin; TAX, paclitaxel; VIN, vinblastine. **p < 0.01, ***p < 0.001 versus control group. Effect of **FC77** on cell cycle distribution towards HL-60 (B) and HCT-116 cells (C) at different time points (1 h, 3 h, 6 h, 9 h, 12 h) with concentrations of corresponding GI_{50}s (HL60, 2.8 nM; HCT-116, 1 nM). *p<0.05, **p<0.01, ***p<0.001 versus G2/M phase of control group. All the experiments are triplicated.

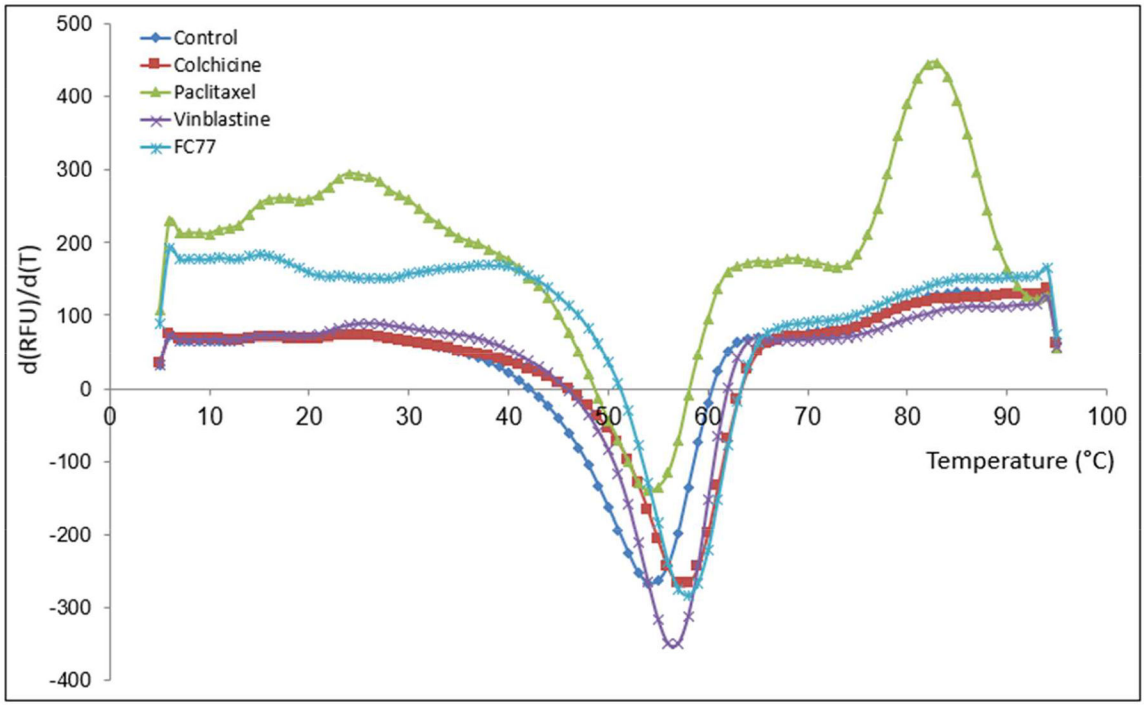

Control	Paclitaxel	Colchicine	Vinblastine	FC77
54	55	57	56	58

Fig. 6.

Thermal shifts in the tubulin monomer (in the presence of GDP, 0.1 mg/mL) with colchicine, paclitaxel, vinblastine or **FC77** (50 μM), as determined by differential scanning fluorimetry. Control: General tubulin buffer (PEM) containing 80 mM PIPES pH 6.9, 2 mM $MgCl_2$ and 0.5 mM EGTA. The melting temperatures of tubulin (°C) with different treatments are presented in the table.

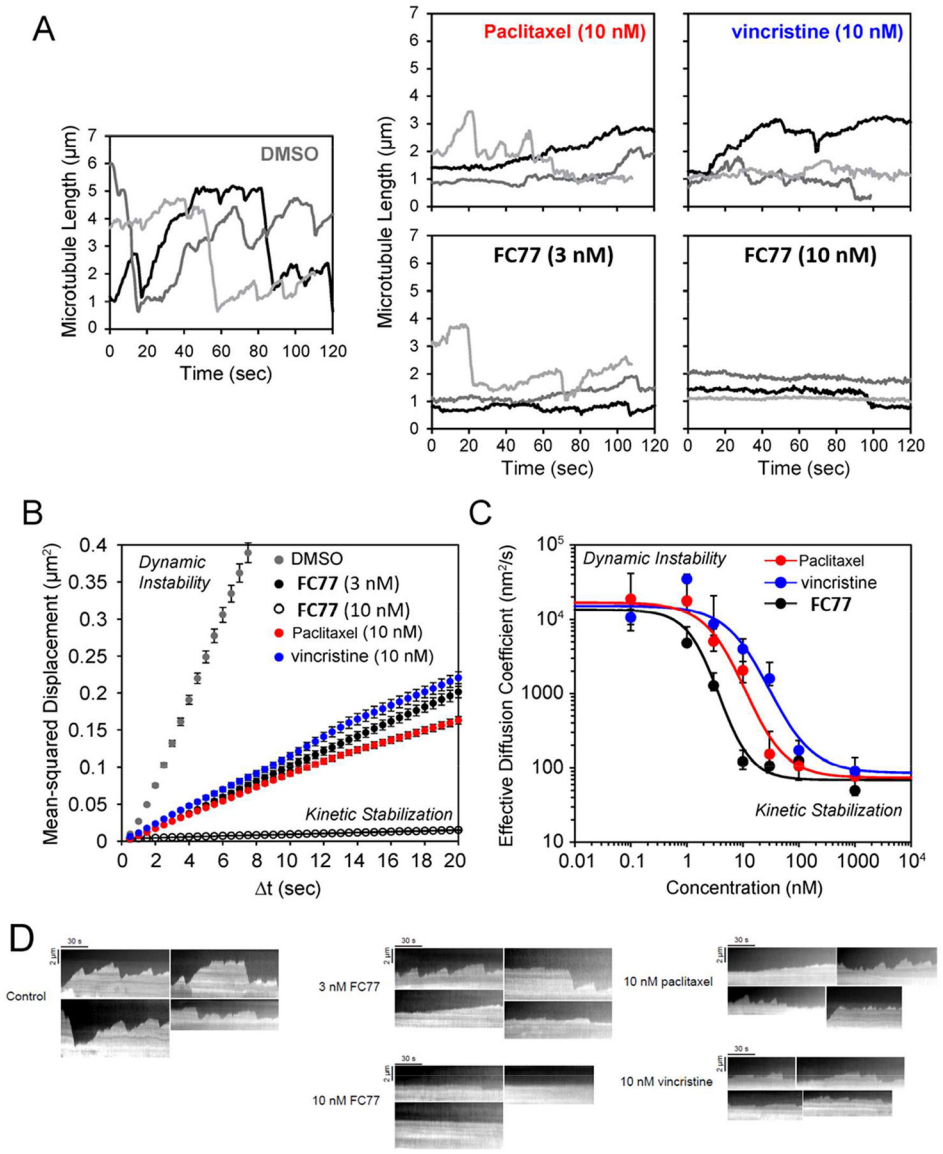

Fig. 7.

Effects of paclitaxel, vincristine, and **FC77** on the microtubule dynamics in LLC-PK1 cells. (**A**) Representative plots of the changes in the microtubule length over time under different conditions. Each trace represents an individual microtubule. (**B**) Mean-squared displacement of the microtubule dynamic end per unit of time. Microtubules undergoing dynamic instability exhibit large displacements (DMSO), while those that are kinetically stabilized or have lost the dynamics exhibit small displacements over time (10 nM **FC77**). Data are presented as the mean ± standard error of the mean. (**C**) Effective diffusion coefficients of the microtubule dynamic end as a function of the concentration of paclitaxel (red), vincristine (blue), and **FC77** (black). Effective diffusion coefficients were estimated from the mean-squared displacements of the dynamic end shown in (**B**). The IC_{50} values were approximately 3 nM for **FC77**, 14 nM for paclitaxel, and 37 nM for vincristine. The best-fit sigmoid curves were obtained for all estimated diffusion coefficients. The diffusion

coefficient data for paclitaxel is from our previous study[22]. (**D**) Microtubule dynamics in the presence of paclitaxel, vincristine, and **FC77**. Representative kymographs of the EGFP–tubulin signal are shown for individual microtubules under the indicated conditions. For each kymograph, the microtubule is aligned to the vertical axis, while time is plotted on the horizontal axis.

Table 1

The 72-h cytotoxicity profile of **FC77** against the NCI-60 cancer cell line panel.

Cell line	GI_{50} (nM)	Cell line	GI_{50} (nM)	Cell line	GI_{50} (nM)	Cell line	GI_{50} (nM)
Leukemia		**Colon cancer**		**CNS cancer**		A498	2.5
CCRF-CEM	5.1	COLO 205	3.5	SF-268	5.5	ACHN	6.2
Hl-60 (TB)	2.3	HCC-2998	4.3	SF-295	3.0	CAKI-1	4.2
K562	3.5	HCT-116	3.6	SF-539	2.8	RXF 393	N.D.
MOLT-4	5.5	HCT-15	3.4	SNB-19	4.1	TK-10	> 100
PRMI-8226	4.8	HT29	4.0	SNB-75	3.3	UO-31	7.9
SR	3.3	KM12	3.6	U251	4.4	**Prostate cancer**	
Non-small-cell lung cancer		SW-620	4.2	**Ovarian cancer**		PC-3	7.9
A549/ATCC	4.1	**Melanoma**		IGROV1	5.6	DU-145	3.8
EKVX	5.2	LOX IMVI	4.7	OVCAR-3	3.3	**Breast cancer**	
HOP-62	5.4	MALME-3M	> 100	OVCAR-4	25.1	MCF-7	3.5
HOP-92	74.1	M14	3.4	OVCAR-5	85.1	MDA-MB-231/ATCC	3.9
NCI-H226	6.2	MDA-MB-435	2.3	OVCAR-8	3.5	HS 578T	4.8
NCI-H23	5.1	SK-MEL-2	12.3	NCI/ADR-RES	3.2	BT-549	5.9
NCI-H460	3.7	SK-MEL-28	17.4	SK-OV-3	7.8	T-47D	N.D.
NCI-H522	2.8	SK-MEL-5	4.3	**Renal cancer**		MDA-MB-468	3.3
		UACC-257	> 100	786–0	6.5		

CNS, central nervous system; GI_{50}, concentration causing 50% inhibition of the cell growth; NCI, National Cancer Institute; N.D., not determined.

Table 2

The top antimicrotubule agents with cancer cell growth inhibitory patterns similar to that of **FC77**.

Name	PCC
Colchicine	0.658
Epothilone A	0.567
Epothilone D	0.564
Docetaxel	0.555
Vincristine	0.547

PCC, Pearson's correlation coefficient.